A Novel Sparsity Measure for Tensor Recovery

Qian Zhao[1] Deyu Meng[1,2,*] Xu Kong[3] Qi Xie[1] Wenfei Cao[1] Yao Wang[1] Zongben Xu[1,2]
[1]School of Mathematics and Statistics, Xi'an Jiaotong University
[2]Ministry of Education Key Lab of Intelligent Networks and Network Security, Xi'an Jiaotong University
[3]School of Mathematical Sciences, Liaocheng University
timmy.zhaoqian@gmail.com dymeng@mail.xjtu.edu.cn xu.kong@hotmail.com
xq.liwu@stu.xjtu.edu.cn {caowenf2015, yao.s.wang}@gmail.com zbxu@mail.xjtu.edu.cn

Abstract

In this paper, we propose a new sparsity regularizer for measuring the low-rank structure underneath a tensor. The proposed sparsity measure has a natural physical meaning which is intrinsically the size of the fundamental Kronecker basis to express the tensor. By embedding the sparsity measure into the tensor completion and tensor robust PCA frameworks, we formulate new models to enhance their capability in tensor recovery. Through introducing relaxation forms of the proposed sparsity measure, we also adopt the alternating direction method of multipliers (ADMM) for solving the proposed models. Experiments implemented on synthetic and multispectral image data sets substantiate the effectiveness of the proposed methods.

1. Introduction

Visual data from real applications are often generated by the interaction of multiple factors. For example, a hyperspectral image consists of a collection of images scattered over various discrete bands and thus includes three intrinsic constituent factors, i.e., spectrum and spatial width and height. Beyond the traditional vector or matrix, which can well address single/binary-factor variability of data, a higher-order tensor, represented as a multidimensional array [24], provides a more faithful representation to deliver the intrinsic structure underlying data ensembles. Due to its comprehensive data-structure-preserving capability, the techniques on tensors have been shown to be very helpful for enhancing the performance of various computer vision tasks, such as multispectral image denoising [33, 52], magnetic resonance imaging recovery [31], and multichannel EEG (electroencephalogram) compression [1].

In real cases, however, due to the acquisition errors conducted by sensor disturbance, photon effects and calibration mistake [1, 31, 37], the tensor data always can only be partially acquired from real data acquisition equipment. Also, some data values could be corrupted by gross noises or outliers [49]. Therefore, recovering tensor from corrupted observations has become a critical and inevitable challenge for tensor data analysis. Such a tensor recovery problem can be formally described in two ways. One is the tensor completion (TC), which focuses on inferring missing entries of the entire tensor from partially observed data; the other is the tensor robust PCA (TRPCA), which corresponds to separating the clean tensor from the corrupting noise. In the degenerated matrix cases, both problems have been thoroughly investigated for decades [7, 23, 34, 35, 42, 6]. However, for general higher-order tensors, until very recent years it begins to attract attention in computer vision and pattern recognition circle [12, 20, 30, 31, 36, 51, 52, 21].

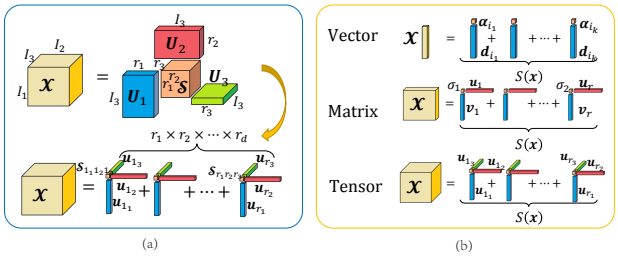

Figure 1. (a) Illustration of Tucker decomposition and its Kronecker representation; (b) Relationship between the proposed sparsity measure and the existing lower-order sparsity measures.

The important clue to handle this issue is to utilize the latent knowledge underlying the tensor structure. The most commonly utilized one is that the tensor intensities along each mode are always with evident correlation. For example, The images obtained across the spectrum of a multispectral image are generally highly correlated. This implies that the tensor along each mode resides on a low-rank subspace and the entire tensor corresponds to the affiliation of the subspaces along all the tensor modes. By fully utilizing such low-rank prior knowledge, the corrupted tensor values

*Corresponding author.

are expected to be properly regularized and faithfully recovered from known ones. This forms the main methodology underlying most of the current tensor recovery methods.

In matrix cases, this low-rank prior is rationally measured by the rank of the training matrix. For practical computation, its relaxations such as the trace norm (also known as nuclear norm) and Schatten-q norm are generally employed. Most current tensor recovery works directly extended this term to higher-order cases by easily ameliorating it as the sum of ranks (or its relaxations) along all tensor modes [30, 31, 9]. Albeit easy to implement, different from matrix scenarios, this simple rank-sum term is short of a clear physical meaning for general tensors. Besides, using same weights to penalize all dimensionality ranks of a tensor is not always rational. Still taking the multispectral image data as example, the tensor intensity along the spectral dimensionality is always significantly more highly correlated than those along the spatial dimensionalities. This prior knowledge delivers the information that the rank of a multispectral image along its spectral dimensionality should be much lower than that along its spatial dimensionalities. We thus should more largely penalize the spectral rank rather than spatial ones.

In this paper, our main argument is that instead of using the sum of tensor ranks along all its modes as conventional, we should more rationally use the multiplication of them to encode the low-rank prior inside the tensor data. This simple measurement can well ameliorate the limitations of the currently utilized ones. Specifically, we can mainly conclude its advantages as follows.

Firstly, it has a natural physical interpretation. As shown in Fig. 1, when the rank of a d-order tensor along its n^{th} mode is r_n, this tensor can be finely represented by at most $\prod_{n=1}^{d} r_n$ Kronecker bases [25, 38][1]. This means that the multiplication of tensor ranks along all its dimensions can be well explained as a reasonable proxy for measuring the capacity of tensor space, in which the entire tensor located, by taking Kronecker basis as the fundamental representation component.

Secondly, it provides a possibly unified way to interpret the sparsity measures throughout vector to matrix. The sparsity of a vector is conventionally measured by the number of the bases (from a predefined dictionary) that can represent the vector as a linear combination of them [8, 14]. Since in vector case, a Kronecker basis is just a common vector, this measurement is just the number of Kronecker bases required to represent the vector, which complies with our proposed sparsity measure. The sparsity of a matrix is conventionally assessed by its rank [7, 34, 42]. Actually there are the following results [15]: (1) if the ranks of a matrix along its two dimensions are r_1 and r_2, respectively, then $r_1 = r_2 = r$; (2) if the matrix is with rank r, then it can be represented as r Kronecker bases. The former result means that the proposed measure (by eliminating the square) is proportional to the conventional one, and the latter indicates that this measure also complies with our physical interpretation.

Thirdly, it provides an insightful understanding for rank weighting mechanism in the traditional rank-sum framework. In specific, since the proposed sparsity measure can be equivalently reformulated as:

$$\prod_{n=1}^{d} r_n = \sum_{n=1}^{d} w_n r_n, \;\; w_n = \frac{1}{d} \prod_{l=1, l\neq n}^{d} r_l,$$

where d is the number of tensor dimensions. In this way, it is easy to see that the subspace located in the tensor dimensionality with lower rank will have a relatively larger weight, and vice versa. E.g., for a hyperspectral image, denote r_s the rank of its spectral dimension and r_w and r_h as ranks of its spatial width and height dimensions. Since generally $r_w, r_h \gg r_s$ in this case, our regularization will more largely penalize r_s (with weight $r_w r_h/3$) than r_w and r_h. This finely accords with the prior knowledge underlying this tensor kind.

In this paper, by embedding this sparsity measure into the TC and TRPCA frameworks, we formulate new models for both issues to enhance their capability in tensor recovery. Throughout the paper, we denote scalars, vectors, matrices and tensors by the non-bold letters, bold lower case letters, bold upper case letters and calligraphic upper case letters, respectively.

2. Related work

Matrix recovery: There are mainly two kinds of matrix recovery problems, i.e., matrix completion (MC) and robust PCA (RPCA), both of which have been extensively studied.

MC problem arises in machine learning scenarios, like collaborative filtering and latent semantic analysis [35]. In 2009, Candès and Recht [7] prompted a new surge for this problem by showing that the matrix can be exactly recovered from an incomplete set of entries through solving a convex semidefinite programming. Similar exact-recovery theory was simultaneously presented by Recht et al. [34], under a certain restricted isometry property, for the linear transformation defined constraints. To alleviate the heavy computational cost, various methods have been proposed to solve the trace norm minimization problem induced by the MC model [4, 23, 26, 28]. Due to the development of these efficient algorithms, MC has been readily applied to computer vision and pattern recognition problems, such as the depth enhancement [32] and image tag completion [18].

RPCA model was initially formulated by Wright et al. [42], with the theoretical guarantee to be able to recover the ground truth tensor from grossly corrupted one under

[1] A Kronecker basis is the simplest rank-1 tensor in the tensor space [5, 24]. For example, in a 2-D case, a Kronecker basis is a rank-1 matrix expressed as the outer product $\mathbf{u}\mathbf{v}^T$ of two vectors $\mathbf{u}$ and $\mathbf{v}$ [15].

certain assumptions [6]. Some variants have been further proposed, e.g., Xu et al. [43] used the $L_{1,2}$-norm to handle data corrupted by column. The iterative thresholding method can be used to solve the RPCA model [6], but is generally slow. To speed up the computation, Lin et al. proposed the accelerated proximal gradient (APG) [27] and the augmented Lagrangian multiplier (ALM) [26] methods. ALM leads to state-of-the-art performance in terms of both speed and accuracy. Bayesian approaches to RPCA have also been investigated. Ding et al. [13] modeled the singular values of the low-rank matrix and the entries of the sparse matrix with beta-Bernoulli priors, and used a Markov chain Monte Carlo (MCMC) sampling scheme to perform inference. Babacan et al. [2] adopted the automatic relevance determination (ARD) approach to RPCA modeling, and utilized the variational Bayes method to do inference.

Tensor recovery: In recent years, tensor recovery have been attracting much attention. Generalized from matrix case, tensor recovery can also be categorized into two lines of researches: tensor completion (TC) and tensor robust PCA (TRPCA). Different from the natural sparsity measure (rank) for matrices, it is more complicated to construct a rational sparsity measure to describe the intrinsic correlations along various tensor modes. By measuring sparsity of a tensor with the sum of the ranks of all unfolding matrices along all modes and relaxing with trace norms, Liu et al. [30] firstly extended the MC model to TC cases and designed efficient HaLRTC algorithm by applying ADMM to solve it [31]. Goldfarb and Qin [21] applied the same sparsity measure to TRPCA problem and also solved it by ADMM. Romera-Paredes and Pontil [36] promoted this "sum of ranks" measure by relaxing it to a tighter convex form. Recently, Zhang et al. [51] proposed a worst case measure, i.e., measuring the sparsity of a tensor by its largest rank of all unfolding matrices, and relaxed it with a sum of exponential forms. Designed mainly for videos, Zhang et al. [52] developed a tensor-SVD based sparsity measure for both TC and TRPCA problems. Xu et al. [44] investigated factorization based method for TC problem.

It can be seen that most of the currently utilized tensor sparsity measures can be recognized as certain relaxations of the sum of the unfolding matrices ranks along all modes. They on one hand lack a clear physical interpretation, and on the other hand have not a consistent relationship with previous defined sparsity measures for vector/matrix. We thus propose a new measure to alleviate this issue.

3. Notions and preliminaries

A tensor corresponds to a multi-dimensional data array. A tensor of order d is denoted as $\mathcal{A} \in \mathbb{R}^{I_1 \times I_2 \times \cdots \times I_d}$. Elements of $\mathcal{A}$ are denoted as $a_{i_1 i_2 \cdots i_d}$, where $1 \leq i_n \leq I_n, 1 \leq n \leq d$. For a d-order tensor $\mathcal{A}$, its n^{th} unfolding matrix is denoted by $\mathbf{A}_{(n)} = \text{unfold}_n(\mathcal{A}) \in \mathbb{R}^{I_n \times (I_1 \cdots I_{n-1} I_{n+1} \cdots I_d)}$, $1 \leq n \leq d$, whose columns compose of all I_n-dimensional vectors along the n^{th} mode of $\mathcal{A}$. Conversely, the unfolding matrix along the n^{th} mode can be transformed back to the tensor by $\mathcal{A} = \text{fold}_n(\mathbf{A}_{(n)})$, $1 \leq n \leq d$. The n-rank of $\mathcal{A}$, denoted as r_n, is the dimension of the vector space spanned by all columns of $\mathbf{A}_{(n)}$.

The product of two matrices can be generalized to the product of a tensor and a matrix. The mode-n product of a tensor $\mathcal{A} \in \mathbb{R}^{I_1 \times \cdots \times I_n \times \cdots I_d}$ by a matrix $\mathbf{B} \in \mathbb{R}^{J_n \times I_n}$, denoted by $\mathcal{A} \times_n \mathbf{B}$, is also an d-order tensor $\mathcal{C} \in \mathbb{R}^{I_1 \times \cdots \times J_n \times \cdots I_N}$, whose entries are computed by

$$c_{i_1 \cdots i_{n-1} j_n i_{n+1} \cdots i_N} = \sum\nolimits_{i_n} a_{i_1 \cdots i_{n-1} i_n i_{n+1} \cdots i_N} b_{j_n i_n}.$$

One important decomposition for tensors is Tucker decomposition [25, 38] (see Fig. 1(a) for visualization), by which any d-order tensor $\mathcal{A} \in \mathbb{R}^{I_1 \times I_2 \times \cdots \times I_d}$ can be written as

$$\mathcal{A} = \mathcal{S} \times_1 \mathbf{U}_1 \times_2 \mathbf{U}_2 \times \cdots \times_d \mathbf{U}_d, \tag{1}$$

where $\mathcal{S} \in \mathbb{R}^{r_1 \times r_2 \times \cdots \times r_d}$ is called the core tensor, and $\mathbf{U}_n \in \mathbb{R}^{I_n \times r_n}$ $(1 \leq n \leq d)$ is composed by the r_n orthogonal bases along the n^{th} mode of $\mathcal{A}$. The Frobenius norm of a tensor $\mathcal{A} = (a_{i_1 \cdots i_d}) \in \mathbb{R}^{I_1 \times \cdots \times I_d}$ is defined as $\|\mathcal{A}\|_F = (\sum_{i_1, \cdots, i_d=1}^{I_1, \cdots, I_d} a_{i_1 \cdots i_d}^2)^{1/2}$, and the L_1 norm is defined as $\|\mathcal{A}\|_1 = \sum_{i_1, \cdots, i_d=1}^{I_1, \cdots, I_d} |a_{i_1 \cdots i_d}|$.

4. New tensor sparsity measure

Our sparsity measure is motivated by the Tucker model of tensors. We know that a d-order tensor $\mathcal{X} \in \mathbb{R}^{I_1 \times I_2 \times \cdots \times I_d}$ can be written as (1). It, as illustrated in Fig. 1(a), can be further rewritten as

$$\mathcal{X} = \sum\nolimits_{i_1, \cdots, i_d=1}^{r_1, \cdots, r_d} s_{i_1 \cdots i_d} \mathbf{u}_{i_1} \circ \mathbf{u}_{i_2} \circ \cdots \circ \mathbf{u}_{i_d},$$

where r_n is the n-rank of $\mathcal{X}$ along its n^{th} mode, and $\mathbf{u}_{i_n}$ is the i_n^{th} column of $\mathbf{U}_n$. In other words, tensor $\mathcal{X}$ can be represented by at most $\prod_{n=1}^{d} r_n$ Kronecker bases. Thus, $\prod_{n=1}^{d} r_n$ provides a natural way to measure the capacity of the tensor space, by taking Kronecker basis as the fundamental representation component. We denote the new tensor sparsity measure as

$$S(\mathcal{X}) = \prod\nolimits_{n=1}^{d} \text{rank}\left(\mathbf{X}_{(n)}\right). \tag{2}$$

Note that $\text{rank}\left(\mathbf{X}_{(n)}\right)$ will lead to combinatorial optimization problems in applications. Therefore, relaxation for $S(\mathcal{X})$ is needed. In matrix case, the tightest convex relaxation for rank is the trace norm, defined as

$$\|\mathbf{X}\|_* = \sum\nolimits_i \sigma_i(\mathbf{X}),$$

where $\sigma_i(\mathbf{X})$ is the n^{th} singular value of the matrix $\mathbf{X}$. Thus, it is natural to relax rank $\left(\mathbf{X}_{(n)}\right)$ to $\|\mathbf{X}_{(n)}\|_*$, and obtain the following relaxation for $S(\mathcal{X})$:

$$S_{\text{trace}}(\mathcal{X}) = \prod\nolimits_{n=1}^{d} \|\mathbf{X}_{(n)}\|_*. \tag{3}$$

Nonconvex relaxations for sparsity measures have also been investigated in literatures [16, 45, 11, 48, 17]. Among them, the so-called folded-concave penalties, such as SCAD [16] and MCP [48] have been shown to have nice statistical properties, and have been successfully applied to matrix or tensor recovery problems [40, 29, 9]. Motivated by these, we also relax the proposed tensor sparsity measure using two folded-concave penalties as follows:

$$S_{\text{mcp}}(\mathcal{X}) = \prod_{n=1}^{d} P_{\text{mcp}}\left(\mathbf{X}_{(n)}\right), \tag{4}$$

and

$$S_{\text{scad}}(\mathcal{X}) = \prod_{n=1}^{d} P_{\text{scad}}\left(\mathbf{X}_{(n)}\right), \tag{5}$$

where

$$P_{\text{mcp}}(\mathbf{X}) = \sum\nolimits_i \psi_{\text{mcp}}(\sigma_i(\mathbf{X})), \;\; P_{\text{scad}}(\mathbf{X}) = \sum\nolimits_i \psi_{\text{scad}}(\sigma_i(\mathbf{X})),$$

with

$$\psi_{\text{mcp}}(t) = \begin{cases} \lambda|t| - \frac{t^2}{2a}, & \text{if } |t| < a\lambda \\ a\lambda^2/2, & \text{if } |t| \geq a\lambda, \end{cases}$$

and

$$\psi_{\text{scad}}(t) = \begin{cases} \lambda|t|, & \text{if } |t| \leq \lambda \\ \frac{a\lambda|t| - 0.5(|t|^2+\lambda^2)}{a-1}, & \text{if } \lambda < |t| < a\lambda \\ \frac{\lambda^2(a^2-1)}{2(a-1)}, & \text{if } |t| \geq a\lambda, \end{cases}$$

respectively. Here, λ and a are the parameters involved of the folded concave penalties, and are empirically specified as 1 and 6 in our experiments.

4.1. Relation to lower-order sparsity measures

Here we briefly discuss the relationship between the proposed tensor sparsity measure and the existing lower-order sparsity measures, as illustrated in Fig. 1(b).

We know that a one-order tensor, i.e., a vector $\mathbf{x}$, can be represented as a linear combination of atoms (one-order Kronecker bases) from a dictionary:

$$\mathbf{x} = \mathbf{D}\boldsymbol{\alpha} = \sum\nolimits_i \alpha_i \mathbf{d}_i, \tag{6}$$

where $\mathbf{D} = (\mathbf{d}_1, \cdots, \mathbf{d}_n)$ is the predefined dictionary and $\boldsymbol{\alpha} = (\alpha_1, \cdots, \alpha_n)^T$ is the coefficients to represent $\mathbf{x}$. In applications, we often seek the $\boldsymbol{\alpha}$ with least sparsity $\|\boldsymbol{\alpha}\|_0$, i.e., with the least non-zero elements, which corresponds to the least Kronecker bases used to represent $\mathbf{x}$.

A two-order tensor, i.e., a matrix, can be represented as the following singular value decomposition (SVD) form:

$$\mathbf{X} = \mathbf{U}\boldsymbol{\Sigma}\mathbf{V}^T = \sum\nolimits_i \sigma_i \mathbf{u}_i \mathbf{v}_i^T, \tag{7}$$

where $\mathbf{U}$ and $\mathbf{V}$ are orthogonal matrices, and $\boldsymbol{\Sigma} = \text{diag}(\boldsymbol{\sigma})$ with $\boldsymbol{\sigma} = (\sigma_1, \cdots, \sigma_n)^T$ being the singular values of $\mathbf{X}$. The sparsity measure of $\mathbf{X}$ is known as its rank, i.e., the number of non-zero elements of $\boldsymbol{\sigma}$. This sparsity intrinsically corresponds to the number of two-order Kronecker bases $\mathbf{u}_i\mathbf{v}_i^T$ used to represent $\mathbf{X}$, and thus also complies with our definition for general tensors.

From the above discussion, we can see that our tensor sparsity measure provides a possibly unified way to interpret the sparsity measures throughout vector to matrix.

It should be noted that the atomic norm [10] provides a similar unification in a more mathematically rigorous way. However, it corresponds to the conventional rank for tensors, which is generally intractable in practice. In contrast, the proposed sparsity measure is based on the Tucker model, and thus can be easily computed.

5. Application to tensor recovery

5.1. Tensor completion

Tensor completion (TC) aims to recover the tensor corrupted by missing values from incomplete observations. Using the proposed sparsity measure, we can mathematically formulate the TC model as

$$\min\nolimits_{\mathcal{X}} \; S(\mathcal{X}), \quad s.t. \;\; \mathcal{X}_\Omega = \mathcal{T}_\Omega, \tag{8}$$

where $\mathcal{X}, \mathcal{T} \in \mathbb{R}^{I_1 \times I_2 \times \cdots \times I_d}$ are the reconstructed and observed tensors, respectively, and the elements of $\mathcal{T}$ indexed by Ω are given while the remaining are missing; $S(\cdot)$ is the tensor sparsity measure as defined in (2). We refer to the model as rank product tensor completion or RP-TC.

In practice, we do not directly adopt model (8), since $S(\mathcal{X})$ makes the optimization difficult to solve. Instead, applying relaxations (3)-(5) to $S(\mathcal{X})$, we can get the following three TC models:

$$\min\nolimits_{\mathcal{X}} \; \tfrac{1}{C_1} S_{\text{trace}}(\mathcal{X}), \quad s.t. \;\; \mathcal{X}_\Omega = \mathcal{T}_\Omega, \tag{9}$$

$$\min\nolimits_{\mathcal{X}} \; \tfrac{1}{C_2} S_{\text{mcp}}(\mathcal{X}), \quad s.t. \;\; \mathcal{X}_\Omega = \mathcal{T}_\Omega, \tag{10}$$

$$\min\nolimits_{\mathcal{X}} \; \tfrac{1}{C_3} S_{\text{scad}}(\mathcal{X}), \quad s.t. \;\; \mathcal{X}_\Omega = \mathcal{T}_\Omega, \tag{11}$$

where C_i $(i = 1, 2, 3)$ are taken for computational convenience (we will discuss this later). We denote the three models as RP-TC$_{\text{trace}}$, RP-TC$_{\text{mcp}}$ and RP-TC$_{\text{scad}}$, respectively.

The above TC models are not convex, and therefore more difficult to solve. Fortunately, we can apply the alternating direction method of multipliers (ADMM) [3, 28] to them. By virtue of ADMM, the original models can be divided into simpler subproblems with closed-form solutions, and thus be effectively solved. To do this, taking RP-TC$_{\text{trace}}$ model (9) as an example, we need to first introduce d auxiliary tensors $\mathcal{M}_n$ $(1 \leq n \leq d)$ and equivalently reformulate the problem as follows:

$$\begin{aligned} &\min_{\mathcal{X}, \mathcal{M}_1, \cdots, \mathcal{M}_d} \frac{1}{C_1} \prod\nolimits_{n=1}^{d} \|\mathbf{M}_{n(n)}\|_* \\ &s.t., \; \mathcal{X}_\Omega = \mathcal{M}_\Omega, \; \mathcal{X} = \mathcal{M}_n, \; 1 \leq n \leq d, \end{aligned} \tag{12}$$

where $\mathbf{M}_{n(n)} = \text{unfold}_n(\mathcal{M}_n)$. Then we consider the augmented Lagrangian function for (12) as:

$$\begin{aligned} &L_\rho(\mathcal{X}, \mathcal{M}_1, \cdots, \mathcal{M}_d, \mathcal{Y}_1, \cdots, \mathcal{Y}_d) \\ &= \frac{1}{C_1} \prod\nolimits_n \|\mathbf{M}_{n(n)}\|_* + \sum\nolimits_n \langle \mathcal{X} - \mathcal{M}_n, \mathcal{Y}_n \rangle + \frac{\rho}{2} \sum\nolimits_n \|\mathcal{X} - \mathcal{M}_n\|_F^2, \end{aligned}$$

where $\mathcal{Y}_n$ $(1 \leq n \leq d)$ are the Lagrange multipliers and ρ is a positive scalar. Now we can solve the problem within the ADMM framework. With $\mathcal{M}_l$ $(l \neq n)$ fixed, $\mathcal{M}_n$ can be updated by solving the following problem:

$$\min_{\mathcal{M}_n} L_\rho(\mathcal{X}, \mathcal{M}_1, \cdots, \mathcal{M}_d, \mathcal{Y}_1, \cdots, \mathcal{Y}_d), \tag{13}$$

which has the closed-form solution:

$$\mathcal{M}_n = \text{fold}_n \left(\text{D}_{\frac{\alpha_n}{\rho}} \left(\text{unfold}_n \left(\mathcal{X} + \frac{1}{\rho} \mathcal{Y}_n \right) \right) \right), \tag{14}$$

where $\text{D}_\tau(\mathbf{X}) = \mathbf{U}\mathbf{\Sigma}_\tau\mathbf{V}^T$ is a shrinkage operator with $\mathbf{\Sigma}_\tau = \text{diag}(\max(\sigma_i(\mathbf{X}) - \tau, 0))$, and

$$\alpha_n = \frac{1}{C_1} \prod_{l=1, l\neq n}^{d} ||\mathbf{M}_{l(l)}||_*, \ 1 \leq n \leq d. \tag{15}$$

Similarly, with $\mathcal{M}_n$s fixed, $\mathcal{X}$ can be updated by solving

$$\min_{\mathcal{X}} \ L_\rho(\mathcal{X}, \mathcal{M}_1, \cdots, \mathcal{M}_d, \mathcal{Y}_1, \cdots, \mathcal{Y}_d), \tag{16}$$

which also has the closed-form solution:

$$\mathcal{X} = \frac{1}{\rho d} \sum_{n=1}^{d} (\rho \mathcal{M}_n - \mathcal{Y}_n). \tag{17}$$

Then the Lagrangian multipliers are updated by

$$\mathcal{Y}_n := \mathcal{Y}_n - \rho(\mathcal{M}_n - \mathcal{X}), \ 1 \leq n \leq d, \tag{18}$$

and ρ is increased to $\mu\rho$ with some constant $\mu > 1$. Note that the above procedure and its derivation are similar to HaLRTC in [31]. The main difference is that the α_i in our algorithm can be varied during the iterations instead of fixed, and thus adaptively give proper penalizations along each mode. This, from the algorithm point of view, explains the advantage of our method beyond previous work.

For models (10) and (11), the general ADMM framework can also be applied. However, due to the more complex folded-concave penalties, we need to slightly modify the algorithm. We leave details in supplementary material. Since models (9)-(11) are not convex, the algorithm can not be guaranteed to achieve global optima, but empirically perform well in all our experiments.

5.2. Tensor robust PCA

Tensor robust PCA (TRPCA) aims to recover the tensor from grossly corrupted observations. The observed tensor can then be written in the following form:

$$\mathcal{T} = \mathcal{L} + \mathcal{E}, \tag{19}$$

where $\mathcal{L}$ is the main tensor with higher-order sparsity, and $\mathcal{E}$ corresponds the sparse noise/outliers embedded in data. Using the proposed tensor sparsity measure, we can get the following TRPCA model:

$$\min_{\mathcal{L},\mathcal{E}} \ S(\mathcal{L}) + \lambda\|\mathcal{E}\|_1, \quad s.t. \ \mathcal{T} = \mathcal{L} + \mathcal{E}, \tag{20}$$

where λ is a tuning parameter compromising the recovery tensor and noise terms.

However, for real data such as hyperspectral image [49], the embedded noise is always not solely sparse, but probably a mixture of sparse and Gaussian. We thus ameliorate the observation expression as:

$$\mathcal{T} = \mathcal{L} + \mathcal{E} + \mathcal{N}, \tag{21}$$

where $\mathcal{N}$ denotes the Gaussian noise. We then propose the following TRPCA model, called rank product TRPCA (RP-TRPCA):

$$\min_{\mathcal{L},\mathcal{E}} \ S(\mathcal{L}) + \lambda\|\mathcal{E}\|_1 + \gamma\|\mathcal{T} - (\mathcal{L} + \mathcal{E})\|_F^2, \tag{22}$$

where γ is the tuning parameter related to the intensity of Gaussian noise. Replacing $S(\mathcal{L})$ with the three relaxations proposed in Section 4, we obtain the following TRPCA models:

$$\min_{\mathcal{L},\mathcal{E}} \ \tfrac{1}{C_1} S_{\text{trace}}(\mathcal{L}) + \lambda\|\mathcal{E}\|_1 + \gamma\|\mathcal{T} - (\mathcal{L}+\mathcal{E})\|_F^2, \tag{23}$$

$$\min_{\mathcal{L},\mathcal{E}} \ \tfrac{1}{C_2} S_{\text{mcp}}(\mathcal{L}) + \lambda\|\mathcal{E}\|_1 + \gamma\|\mathcal{T} - (\mathcal{L}+\mathcal{E})\|_F^2, \tag{24}$$

$$\min_{\mathcal{L},\mathcal{E}} \ \tfrac{1}{C_3} S_{\text{scad}}(\mathcal{L}) + \lambda\|\mathcal{E}\|_1 + \gamma\|\mathcal{T} - (\mathcal{L}+\mathcal{E})\|_F^2, \tag{25}$$

which are referred as RP-TRPCA$_{\text{trace}}$, RP-TRPCA$_{\text{mcp}}$ and RP-TRPCA$_{\text{scad}}$, respectively.

Similar to the TC case, we also apply the ADMM to solving these models. Taking RP-TRPCA$_{\text{trace}}$ model (23) as an example, by introducing auxiliary tensors $\mathcal{M}_n$ $(1 \leq n \leq d)$, we can equivalently reformulate it as:

$$\begin{aligned} \min_{\mathcal{L},\mathcal{E}\mathcal{M}_1,\cdots,\mathcal{M}_d} & \frac{1}{C_1} \prod_{n=1}^{d} \|\mathbf{M}_{n(n)}\|_* + \lambda\|\mathcal{E}\|_1 + \gamma\|\mathcal{T} - (\mathcal{L}+\mathcal{E})\|_F^2 \\ s.t., \ & \mathcal{L} = \mathcal{M}_n, \ 1 \leq n \leq d. \end{aligned} \tag{26}$$

Then the augmented Lagrangian function for (26) becomes

$$\begin{aligned} & L_\rho(\mathcal{L}, \mathcal{E}, \mathcal{M}_1, \cdots, \mathcal{M}_d, \mathcal{Y}_1, \cdots, \mathcal{Y}_d) \\ & = \frac{1}{C_1} \prod_n \|\mathbf{M}_{n(n)}\|_* + \lambda\|\mathcal{E}\|_1 + \gamma\|\mathcal{T} - (\mathcal{L}+\mathcal{E})\|_F^2 \\ & \quad + \sum\nolimits_n \langle \mathcal{X} - \mathcal{M}_n, \mathcal{Y}_n \rangle + \frac{\rho}{2} \sum\nolimits_n \|\mathcal{X} - \mathcal{M}_n\|_F^2. \end{aligned}$$

Within the ADMM framework, the original problem can be solved via alternatively solving a sequence of subproblems with respect to L_ρ. Besides, all the subproblems involved can be efficiently solved similar to solving RP-TC models. We omit the details due to space limitations

5.3. Discussion for setting C_i

Now we briefly discuss how to determine the parameter C_i involved in the proposed TC and TRPCA models. For the TC models, since there is only one term in the objective function, C_i mainly guarantees the computation stability. Therefore, we can fix it as a relative large constant. In the TRPCA models, the situation is more complicated, since there are three terms in the objective function, and C_i, together with λ and γ, balances these terms. We empirically found that the algorithm performs consistently well under the setting $C_i = \frac{1}{d} \sum_{n=1}^{d} \prod_{l\neq n} P(\mathbf{L}_{(l)})$, λ to be with order

of $1/\sqrt{\max\{I_i\}_{n=1}^{d}}$ and $\gamma = 0.1/\sigma$, where $\mathbf{L}_{(l)}$ is the l^{th} unfolding matrix of the ground truth tensor $\mathcal{L}$, $P(\cdot)$ corresponds to the matrix sparsity measure and σ is the standard deviation of the Gaussian noise. Since the ground truth tensor $\mathcal{L}$ is unknown, we first run another easy-to-be-implemented TRPCA method, such as that proposed in [21], to initialize C_i based on the obtained result, and then implement our algorithms under such initialization. This strategy performs well throughout our experiments.

6. Experiments

In this section, we evaluate the effectiveness of the proposed sparsity measure for tensor recovery problems, including TC and TRPCA, on both synthetic and real data. All experiments were implemented in Matlab 8.4(R2014b) on a PC with 3.50GHz CPU and 32GB RAM.

6.1. Tensor completion experiments

Synthetic tensor completion. The synthetic data were generated as follows: first, the ground truth tensor was yielded from the Tucker model, i.e., $\mathcal{T} = \mathcal{S} \times_1 \mathbf{U}_1 \times_2 \mathbf{U}_2 \times_3 \mathbf{U}_3$, where the core tensor $\mathcal{S} \in \mathbb{R}^{r_1 \times r_2 \times r_3}$ was randomly generated from the standard Gaussian distribution, and all $\mathbf{U}_n \in \mathbb{R}^{I_n \times r_n}$ were randomly generated column-orthogonal matrices; then a portion of elements was randomly sampled as observed data while the rest were left as missing components. We set I_n $(n = 1, \cdots, 3)$ to 50, respectively, resulting the ground truth tensor with size $50 \times 50 \times 50$. For the rank parameters r_n along each mode, we considered two settings, $(10, 20, 40)$ and $(20, 40, 40)$. These settings are designed to simulate the ranks along different modes with diversity, which is always encountered in practice, e.g., for multispectral image, the rank along the spectral mode is always much lower than those along the spatial modes[2]. We then varied the percentage of sampled elements from 20% to 80% and reconstructed the tensor using the proposed methods and the state-of-the-arts along this line, including ALM based matrix completion (denoted as MC-ALM) [26], HaLRTC [31], McpLRTC [9], ScadLRTC [9], tensor-SVD based TC method (t-SVD) [52] and factorization based TC method (TMac) [44]. The performance in terms of *relative reconstruction error* (RRE)[3], averaged over 20 realizations, was summarized in Table 1. For matrix-based method MC-ALM, we applied it to the unfolded matrix along each mode of the tensor, obtaining 3 RREs, and report the best one. The average computation time are also listed.

[2]We have also tried the setting that all the modes are with the same rank as mostly investigated in previous work [20, 30, 31], while most of the methods, including ours, perform similarly well. Therefore, we do not include the results to save space.

[3]Defined as $\text{RRE} = \|\mathcal{X} - \mathcal{T}\|_F / \|\mathcal{T}\|_F$, where $\mathcal{T}$ and $\mathcal{X}$ denote the ground truth and reconstructed tensors, respectively.

Table 1. Performance comparison of 9 competing TC methods on synthetic data with rank setting (10, 20, 40) (upper) and (20, 40, 40) (lower). The best and the second best results in terms of RRE are highlighted in bold with and without underline, respectively.

Method	20%	30%	40%	80%	Avg. Time (s)
MC-ALM [26]	0.567	0.306	5.54e-2	1.76e-8	1.18
HaLRTC [31]	0.835	0.704	0.543	2.46e-8	1.42
t-SVD [52]	0.815	0.628	0.427	1.48e-4	21.5
TMac [44]	4.05e-3	1.44e-3	6.95e-4	1.80e-4	1.58
McpLRTC [9]	2.93e-5	2.26e-8	7.85e-12	5.23e-16	14.43
ScadLRTC [9]	2.94e-5	2.26e-8	7.85e-12	5.23e-16	14.46
RP-TC$_{\text{trace}}$	0.833	0.697	0.517	1.52e-8	5.70
RP-TC$_{\text{mcp}}$	**9.30e-6**	**4.70e-9**	**1.89e-12**	**5.20e-16**	18.23
RP-TC$_{\text{scad}}$	**9.28e-6**	**4.28e-9**	**9.78e-13**	**5.18e-16**	18.07
Method	20%	30%	40%	80%	Avg. Time (S)
MC-ALM [26]	**0.783**	0.646	0.503	1.36e-7	0.72
HaLRTC [31]	0.875	0.794	0.703	0.160	0.73
t-SVD [52]	0.937	0.838	0.726	9.72e-2	7.51
TMac [44]	0.943	0.192	5.55e-3	3.31e-4	2.83
McpLRTC [9]	0.973	0.498	1.85e-4	2.57e-14	10.63
ScadLRTC [9]	0.973	0.498	1.85e-4	2.57e-14	10.59
RP-TC$_{\text{trace}}$	0.875	0.793	0.701	0.119	2.89
RP-TC$_{\text{mcp}}$	0.836	**7.05e-4**	**6.86e-5**	**1.70e-14**	12.86
RP-TC$_{\text{scad}}$	**0.833**	**5.23e-4**	**6.85e-5**	**1.74e-14**	12.85

It can be seen from Table 1 that, compared with other competing methods, the proposed RP-TC$_{\text{mcp}}$ and RP-TC$_{\text{scad}}$ methods can accurately recover the tensor with very few observations (20% or 30%). Specifically, under the rank setting $(10, 20, 40)$, the proposed methods, together with three other methods can recover the tensor with 20% observations, and the proposed methods perform slightly better than the methods in [9]. Under the more challenging rank setting $(20, 40, 40)$, all methods failed with 20% observations, while only the proposed methods can accurately recover the ground truth tensor with 30% elements observed. It is also observed that RP-TC$_{\text{trace}}$ does not perform very well in this tensor completion task. This is due to the fact that, as a relaxation for the rank of the unfolding matrix, trace norm is not so tight, and thus makes the relaxation for the proposed sparsity measure even looser.

As for computational cost, we can see that the proposed methods with folded-concave relaxations have similar amount of running time as the methods in [9], which also used folded-concave penalties. Considering their better performance, the cost is acceptable.

Multispectral image completion. Then we test the performance of the proposed methods using multispectral image data. Two well-known data sets, Natural Scenes 2002 [19][4] and Columbia Multispectral Image Database [46][5], were considered. The former contains multispectral images captured from 8 scenes, with 31 bands (varying wavelength from 410nm to 710nm in 10nm steps) and spatial resolution 820×820 natural scene; the latter contains 32 real-world scenes, each with spatial resolution 512×512 and 31 bands (varying from 400nm to 700nm in 10nm steps).

We used 2 images from Natural Scenes 2002 (*Scene 4*

[4]http://personalpages.manchester.ac.uk/staff/d.h.foster/

[5]http://www1.cs.columbia.edu/CAVE/databases/multispectral/

Table 2. The average performance comparison of 9 competing TC methods with different sampling rates on 8 multispectral images.

Method	10%					20%					50%					Avg. Time (s)	
	PSNR	SSIM	FSIM	ERGAS	SAM	PSNR	SSIM	FSIM	ERGAS	SAM	PSNR	SSIM	FSIM	ERGAS	SAM	Columbia	Natural Scenes
MC-ALM [26]	25.46	0.650	0.817	275.7	0.253	28.72	0.776	0.882	195.4	0.190	35.51	0.936	0.963	91.0	0.0999	30.1	123.1
HaLRTC [31]	26.58	0.710	0.824	258.4	0.210	30.98	0.836	0.905	163.9	0.147	39.98	0.968	0.981	61.3	0.0686	59.6	246.6
t-SVD [52]	31.91	0.849	0.919	137.2	0.188	36.96	0.935	0.964	80.0	0.126	46.42	**0.989**	**0.994**	28.8	0.0515	736.6	2075.1
TMac [44]	30.83	0.752	0.879	171.6	0.239	34.38	0.846	0.918	122.4	0.183	40.97	0.958	0.976	54.8	0.0832	86.7	174.7
McpLRTC [9]	31.55	0.803	0.894	154.1	0.191	35.69	0.897	0.943	98.8	0.134	44.01	0.980	0.989	39.1	0.0574	303.2	908.9
ScadLRTC [9]	31.11	0.774	0.882	172.1	0.224	35.23	0.873	0.931	111.4	0.159	43.72	0.977	0.987	40.7	0.0622	314.2	916.0
RP-TC$_{\text{trace}}$	26.76	0.728	0.835	251.2	0.218	31.80	0.864	0.920	147.8	0.144	42.45	0.983	0.990	43.6	0.0532	112.9	483.2
RP-TC$_{\text{mcp}}$	**35.80**	**0.936**	**0.962**	**81.4**	**0.105**	**41.07**	**0.976**	**0.986**	**46.1**	**0.0629**	**51.74**	**0.998**	**0.999**	**13.6**	**0.0219**	341.9	1117.9
RP-TC$_{\text{scad}}$	**35.70**	**0.933**	**0.961**	**81.9**	**0.107**	**40.48**	**0.973**	**0.984**	**48.6**	**0.0650**	**51.40**	**0.998**	**0.999**	**14.2**	**0.0229**	390.6	1126.3

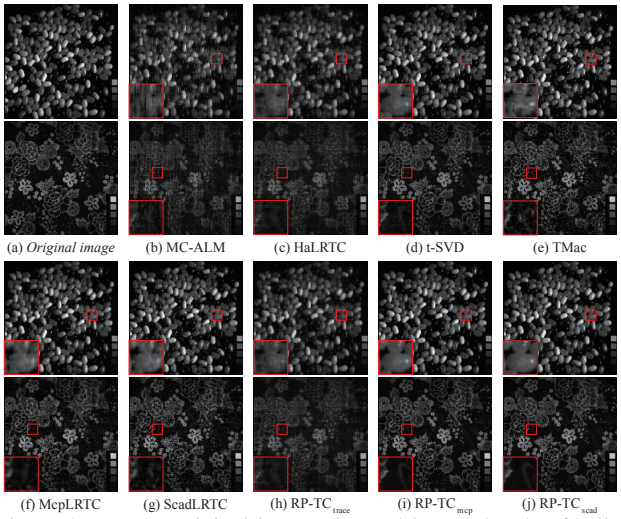

(a) *Original image* (b) MC-ALM (c) HaLRTC (d) t-SVD (e) TMac

(f) McpLRTC (g) ScadLRTC (h) RP-TC$_{\text{trace}}$ (i) RP-TC$_{\text{mcp}}$ (j) RP-TC$_{\text{scad}}$

Figure 2. (a) The original images located in two bands of *jellybeans* and *cloth*; (b)-(j) The recovered images by MC-ALM [26], HaLRTC [31], t-SVD [52], TMac [44], McpLRTC [9], ScadLRTC [9], RP-TC$_{\text{trace}}$, RP-TC$_{\text{mcp}}$ and RP-TC$_{\text{scad}}$, respectively.

and *Scene 8*) and 6 images from Columbia Multispectral Image Database (*balloons*, *beads*, *cloth*, *jelleybeans*, *peppers* and *watercolors*) in our experiments, and each image was downsampled with half length and width of the original one. Then we varied the sampling rate from 10% to 50%, and applied TC methods to recovering the images. Similar to the performance evaluation utilized by Peng et al. [33], we employ the following five quantitative picture quality indices (PQI) to assess the performance of a TC method: peak signal-to-noise ratio (PSNR), structure similarity (SSIM) [41], feature similarity (FSIM) [50], erreur relative globale adimensionnelle de synthèse (ERGAS) [39] and spectral angle mapper (SAM) [47]. Good completion results correspond to larger values in PSNR, SSIM and FSIM, and smaller values in ERGAS and SAM.

The averaged performances of each method over the 8 images under different sampling rates are summarized in Table 2 (detailed results on each image are presented in supplementary material). It can be seen that, in all cases, the proposed RP-TC$_{\text{mcp}}$ and RP-TC$_{\text{scad}}$ outperform other methods in terms of all the PQIs. Even at very low sampling rate (10%), our methods can obtain good recovery of the ground truth images. For running time, similar conclusion can be made as in synthetic tensor completion. Specifically, the proposed methods take similar time as methods in [9], while much faster than t-SVD, which has the best performance excluding our methods.

For visually comparison, we use two bands of *jellybeans* and *cloth* images with 20% sampling rate to demonstrate the completion results by the 9 competing methods, as shown in Fig. 2. We can see that RP-TC$_{\text{mcp}}$ and RP-TC$_{\text{scad}}$ get evidently better recovery. Specifically, more details of the texture, edge and surface are recovered by our methods.

6.2. Tensor robust PCA

Simulated multispectral image restoration. We first test the proposed TRPCA models by restoring multispectral images corrupted by artificially added noise. The idea is motivated by the application of low-rank matrix based method to image denoising [22]. In [22], Gu et al. proposed an image denoising method by exploiting the low-rank property of the matrix formed by nonlocal similar patches. Compared with gray image studied there, multispectral image has an additional spectral dimension. Besides, the different spectral bands are generally highly correlated. Therefore, we can generalize the matrix based denoising method to tensor case using the proposed TRPCA models. The idea is as follows: for a 3D tensor patch, we search for its nonlocal similar patches across the multispectral image, and reshape these patches to matrices; these matrices are then stacked into a new 3D tensor, which is the input of our TRPCA methods for denoising; we further extract the cleaned patches from the output of TRPCA and aggregate them to restore the whole multispectral image.

We used 10 images from Columbia Multispectral Image Database, including *balloons*, *beads*, *chart and stuffed toy*, *cloth*, *egyptian statue*, *feathers*, *flowers*, *photo and face*, *pompoms* and *watercolors*, for testing (more results are presented in supplementary material). Each image is resized to 256×256 for all spectral bands, and rescale to $[0, 1]$. Gaussian noise with standard deviation $\sigma = 0.1$ was added, and 10% of the pixels were further randomly chosen and added to salt-and-pepper noise. Mixing the two kinds of noises aims to simulate real noise that can be found in remote hyperspectral images [49]. We implemented the proposed RP-TRPCA methods, and 3 competing methods, including RPCA [26], HoRPCA [21] and t-SVD [52]. For matrix based RPCA, we only considered the low-rank prop-

Table 3. The average performance comparison of 7 competing methods on 10 noisy multispectral images.

	PSNR	SSIM	FSIM	ERGAS	SAM
Noisy image	13.01	0.116	0.387	1084.9	0.946
TDL [33]	26.03	0.631	0.887	241.4	0.287
RPCA [26]	28.66	0.670	0.836	170.7	0.491
HoRPCA [21]	28.77	0.829	0.880	174.0	0.247
t-SVD [52]	29.81	0.713	0.868	152.9	0.370
RP-TRPCA$_{\text{trace}}$	28.86	**0.832**	0.881	172.5	0.251
RP-TRPCA$_{\text{mcp}}$	**32.50**	**0.832**	**0.922**	**112.9**	**0.237**
RP-TRPCA$_{\text{scad}}$	**32.27**	**0.818**	**0.914**	**116.3**	**0.242**

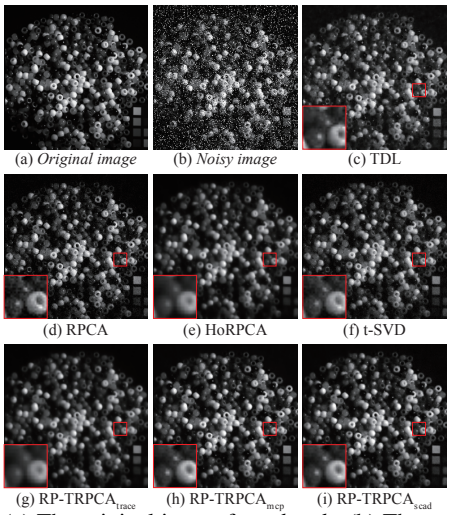

(a) *Original image* (b) *Noisy image* (c) TDL (d) RPCA (e) HoRPCA (f) t-SVD (g) RP-TRPCA$_{\text{trace}}$ (h) RP-TRPCA$_{\text{mcp}}$ (i) RP-TRPCA$_{\text{scad}}$

Figure 3. (a) The original image from *beads*; (b) The corresponding noisy image; (c)-(i) The recovered images by TDL[33], RPCA [26], HoRPCA [21], t-SVD [52], RP-TRPCA$_{\text{trace}}$, RP-TRPCA$_{\text{mcp}}$ and RP-TRPCA$_{\text{scad}}$, respectively.

erty along spectral dimension, since matrix based method can only capture one type of correlation, and the spectral one is generally more preferred in our experiences. For TRPCA based methods, patches extracted were of size 8×8 with step of 2 pixels at each band, and the group size of nonlocal patches was set to 40. We also performed TDL [33], which represents the state-of-the-art for multispectral image denoising with Gaussian noise, as a baseline method. The averaged restoration results in terms of the 5 PQIs mentioned before are summarized in Table 3.

It is easy to see that our methods outperform other methods in terms of all PQIs, which verifies their effectiveness in removing the heavy noise. We also show the restoration results of one band from *beads* image in Fig. 3, which shows that the proposed RP-TRPCA$_{\text{mcp}}$ and RP-TRPCA$_{\text{scad}}$ can recover the image with relatively better visual quality. Note that this experiment is to demonstrate the effectiveness of the proposed models, and the results are only preliminary. If we focus on denoising problem itself, more sophisticated techniques are needed.

Real hyperspectral image restoration. Now we apply the proposed TRPCA models to real hyperspectral image restoration. We used a HYDICE urban image[6] for demonstration. The original image is of size $307 \times 307 \times 210$, while contains several bands seriously polluted by the atmosphere and water absorption. After removing these seriously polluted bands, we obtain the image of size $307 \times 307 \times 188$. Using the similar method described before, we can apply the competing methods to restoring this image. For TRPCA based methods, patches of size 8×8 with step of 4 pixels were extracted, and the group size was set to 20. The restoration results on sample bands are shown in Fig. 4.

[6] http://www.tec.army.mil/hypercube

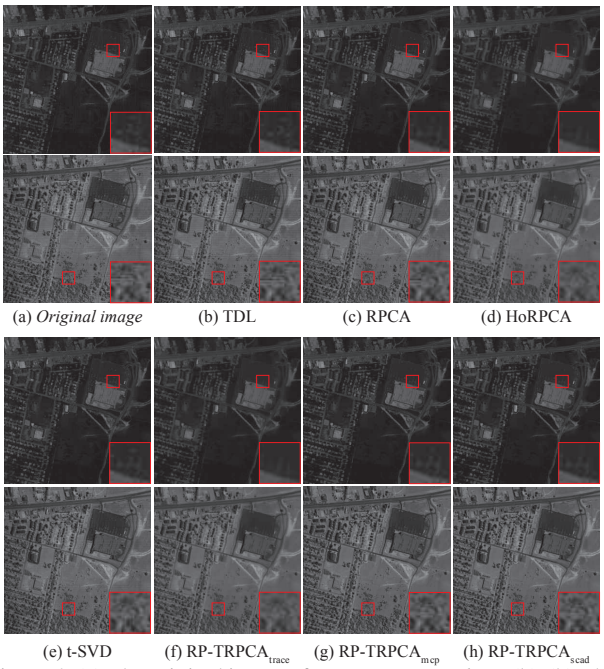

(a) *Original image* (b) TDL (c) RPCA (d) HoRPCA (e) t-SVD (f) RP-TRPCA$_{\text{trace}}$ (g) RP-TRPCA$_{\text{mcp}}$ (h) RP-TRPCA$_{\text{scad}}$

Figure 4. (a) The original images from *HYDICE urban*; (b)-(h) The restored images by MC-ALM [26], HaLRTC [31], t-SVD [52], TMac [44], RP-TC$_{\text{trace}}$, RP-TC$_{\text{mcp}}$ and RP-TC$_{\text{scad}}$, respectively.

It can be seen that, though all of the competing methods can restore the image from the corrupted observations to some degree, most of them either fail to remove the stripes or over-smooth the image with loss of edge and texture information. In contrast, our methods not only completely remove the complex noise embedded in the image, but also faithfully preserve the image details.

7. Conclusion

In this paper, we present a new tensor sparsity measure, together with its three relaxations. Then we apply it to TC and TRPCA models, and design the ADMM algorithms to solve them. The experiments on synthetic and multispectral image data substantiate the rationality of the proposed sparsity measure and the effectiveness of our models on tensor recovery tasks.

Acknowledgments. This research was supported by 973 Program of China with No. 3202013CB329404, and the NSFC projects with No. 61373114, 11401286, 91330204, 11131006, 61503263.

References

[1] E. Acar, D. M. Dunlavy, T. G. Kolda, and M. Mørup. Scalable tensor factorizations for incomplete data. *Chemometrics and Intelligent Laboratory Systems*, 106(1):41–56, 2001.

[2] S. D. Babacan, M. Luessi, R. Molina, and A. K. Katsaggelos. Sparse Bayesian methods for low-rank matrix estimation. *IEEE TSP*, 60(8):3964–3977, 2012.

[3] S. Boyd, N. Parikh, E. Chu, B. Peleato, and J. Eckstein. Distributed optimization and statistical learning via the alternating direction method of multipliers. *Foundations and Trends in Machine Learning*, 3(1):1–122, 2011.

[4] J. F. Cai, E. J. Candès, and Z. Shen. A singular value thresholding algorithm for matrix completion. *SIAM Journal on Optimization*, 20(4):1956–1982, 2010.

[5] C. F. Caiafa and A. Cichocki. Computing sparse representations of multidimensional signals using Kronecker bases. *Neural Computation*, 25(1):186–220, 2013.

[6] E. J. Candès, X. Li, Y. Ma, and J. Wright. Robust principal component analysis? *Journal of the ACM*, 58(3):11:1–11:37, 2011.

[7] E. J. Candès and B. Recht. Exact matrix completion via convex optimization. *Foundations of Computational Mathematics*, 9(6):717–772, 2009.

[8] E. J. Candès, J. Romberg, and T. Tao. Stable signal recovery from incomplete and inaccurate measurements. *Communications on Pure and Applied Mathematics*, 59(8):1207–1223, 2006.

[9] W. Cao, Y. Wang, C. Yang, X. Chang, Z. Han, and Z. Xu. Folded-concave penalization approaches to tensor completion. *Neurocomputing*, 152(0):261 – 273, 2015.

[10] V. Chandrasekaran, B. Recht, P. A. Parrilo, and A. S. Willsky. The convex algebraic geometry of linear inverse problems. *Foundations of Computational Mathematics*, 12(6):805–849, 2012.

[11] R. Chartrand. Exact reconstruction of sparse signals via nonconvex minimization. *IEEE Signal Processing Letters*, 14(10):707–710, 2007.

[12] Y. L. Chen, C.-T. Hsu, and H.-Y. M. Liao. Simultaneous tensor decomposition and completion using factor priors. *IEEE TPAMI*, 36(3):577–591, 2014.

[13] X. Ding, L. He, and L. Carin. Bayesian robust principal component analysis. *IEEE TIP*, 20(12):3419–3430, 2011.

[14] D. Donoho. Compressed sensing. *IEEE TIT*, 52(4):1289–1306, 2006.

[15] C. Eckart and G. Young. The approximation of one matrix by another of lower rank. *Psychometrika*, 1(3):211–218, 1936.

[16] J. Fan and R. Li. Variable selection via nonconcave penalized likelihood and its oracle properties. *Journal of the American Statistical Association*, 96(456):1348–1360, 2001.

[17] J. Fan, L. Xue, and H. Zou. Strong oracle optimality of folded concave penalized estimation. *Annals of Statistics*, 42(3):819–849, 2014.

[18] Z. Y. Feng, S. H. Feng, R. Jin, and A. K. Jain. Image tag completion by noisy matrix recovery. In *ECCV*, 2014.

[19] D. H. Foster, K. Amano, S. Nascimento, and M. J. Foster. Frequency of metamerism in natural scenes. *Journal of the Optical Society of America A*, 23(10):2359–2372, 2006.

[20] S. Gandy, B. Recht, and I. Yamada. Tensor completion and low-n rank tensor recovery via convex optimization. *Inverse Problems*, 27(3):331–336, 2011.

[21] D. Goldfarb and Z. T. Qin. Robust low-rank tensor recovery: Models and algorithms. *SIAM Journal on Matrix Analysis and Applications*, 35(1):225–253, 2014.

[22] S. Gu, L. Zhang, W. Zuo, and X. Feng. Weighted nuclear norm minimization with application to image denoising. In *CVPR*, 2014.

[23] Y. Hu, D. B. Zhang, J. P. Ye, X. L. Li, and X. F. He. Fast and accurate matrix completion via truncated nuclear norm regularization. *IEEE TPAMI*, 35(9):2117–2130, 2013.

[24] T. G. Kolda and B. W. Bader. Tensor decompositions and applications. *SIAM Review*, 51(3):455–500, 2009.

[25] L. D. Lathauwer, B. D. Moor, and J. Vandewalle. A multilinear singular value decomposition. *SIAM Journal on Matrix Analysis and Applications*, 21(4):1253–1278, 2000.

[26] Z. Lin, M. Chen, and Y. Ma. The augmented Lagrange multiplier method for exact recovery of corrupted low-rank matrices. Technical Report UILU-ENG-09-2215, UIUC, 2009.

[27] Z. Lin, A. Ganesh, J. Wright, L. Wu, M. Chen, and Y. Ma. Fast convex optimization algorithms for exact recovery of a corrupted low-rank matrix. Technical Report UILU-ENG-09-2214, UIUC, 2009.

[28] Z. C. Lin, R. S. Liu, and Z. X. Su. Linearized alternating direction method with adaptive penalty for low rank representation. In *NIPS*, 2011.

[29] D. Liu, T. Zhou, H. Qian, C. Xu, and Z. Zhang. A nearly unbiased matrix completion approach. In *ECML/PKDD*, 2013.

[30] J. Liu, P. Musialski, P. Wonka, and J. P. Ye. Tensor completion for estimating missing values in visual data. In *ICCV*, 2009.

[31] J. Liu, P. Musialski, P. Wonka, and J. P. Ye. Tensor completion for estimating missing values in visual data. *IEEE TPAMI*, 34(1):208–220, 2013.

[32] S. Lu, X. F. Ren, and F. Liu. Depth enhancement via low-rank matrix completion. In *CVPR*, 2014.

[33] Y. Peng, D. Y. Meng, Z. B. Xu, C. Q. Gao, Y. Yang, and B. Zhang. Decomposable nonlocal tensor dictionary learning for multispectral image denoising. In *CVPR*, 2014.

[34] B. Recht, M. Fazel, and P. A. Parrilo. Guaranteed minimum-rank solutions of linear matrix equations via nuclear norm minimization. *SIAM Review*, 52(3):471–501, 2010.

[35] J. D. M. Rennie and N. Srebro. Fast maximum margin matrix factorization for collaborative prediction. In *ICML*, 2005.

[36] B. Romera-Paredes and M. Pontil. A new convex relaxation for tensor completion. In *NIPS*, 2013.

[37] M. Signoretto, R. V. de Plas, B. D. Moor, and J. A. K. Suykens. Tensor versus matrix completion: A comparison with application to spectral data. *IEEE Signal Processing Letters*, 18(7):403–406, 2011.

[38] L. R. Tucker. Some mathematical notes on three-mode factor analysis. *Psychometrika*, 31(3):279–311, 1966.

[39] L. Wald. *Data Fusion: Definitions and Architectures: Fusion of Images of Different Spatial Resolutions*. Presses de l'Ecole des Mines, 2002.

[40] S. Wang, D. Liu, and Z. Zhang. Nonconvex relaxation approaches to robust matrix recovery. In *IJCAI*, 2013.

[41] Z. Wang, A. C. Bovik, H. R. Sheikh, and E. P. Simoncelli. Image quality assessment: from error visibility to structural similarity. *IEEE TIP*, 13(4):600–612, 2004.

[42] J. Wright, Y. Peng, Y. Ma, A. Ganesh, and S. Rao. Robust principal component analysis: Exact recovery of corrupted low-rank matrices by convex optimization. In *NIPS*, 2009.

[43] H. Xu, C. Caramanis, and S. Sanghavi. Robust PCA via outlier pursuit. In *NIPS*, 2010.

[44] Y. Xu, R. Hao, W. Yin, and Z. Su. Parallel matrix factorization for low-rank tensor completion. *arXiv preprint arXiv:1312.1254*, 2013.

[45] Z. Xu, X. Chang, F. Xu, and H. Zhang. $L_{1/2}$ regularization: A thresholding representation theory and a fast solver. *IEEE TNNLS*, 23(7):1013–1027, 2012.

[46] F. Yasuma, T. Mitsunaga, and D. Iso. Generalized assorted pixel camera: postcapture control of resolution, dynamic range and spectrum. *IEEE TIP*, 19(9):2241–2253, 2010.

[47] R. H. Yuhas, J. W. Boardman, and A. F. H. Goetz. Determination of semi-arid landscape endmembers and seasonal trends using convex geometry spectral unmixing techniques. In *Summaries of the 4th Annual JPL Airborne Geoscience Workshop*, 1993.

[48] C. Zhang. Nearly unbiased variable selection under minimax concave penalty. *Annals of Statistics*, 38(2):894–942, 2010.

[49] H. Zhang, W. He, L. Zhang, H. Shen, and Q. Yuan. Hyperspectral image restoration using low-rank matrix recovery. *IEEE TGRS*, 52(8):4729–4743, Aug 2014.

[50] L. Zhang, X. Q. Mou, and D. Zhang. Fsim: a feature similarity index for image quality assessment. *IEEE TIP*, 20(8):2378C–2386, 2011.

[51] X. Q. Zhang, Z. Y. Zhou, D. Wang, and Y. Ma. Hybrid singular value thresholding for tensor completion. In *AAAI*, 2014.

[52] Z. M. Zhang, G. Ely, S. Aeron, N. Hao, and M. E. Kilmer. Novel methods for multilinear data completion and de-noising based on tensor-SVD. In *CVPR*, 2014.